28-GHz High-Speed Train Measurements and Propagation Characteristics Analysis

Jae-Joon Park, Juyul Lee, Kyung-Won Kim, and Myung-Don Kim

Electronics and Telecommunications Research Institute (ETRI)
218 Gajeong-ro, Yuseong-gu, Daejeon, 34129, Korea
E-mail: {jjpark, juyul, kimkw, mdkim}@etri.re.kr

***Abstract*—In this paper, we investigate millimeter-wave propagation characteristics of a high-speed moving train based on field measurements in tunnel and viaduct scenarios. The measurements were carried out at 28 GHz, emulating a 3GPP-like high-speed train (HST) deployment scenario where a transmitter is positioned next to a track and a receiver is mounted on the roof of a train carriage. Path loss (PL) and other channel parameters, including delay spread and Doppler shift, were investigated. One interesting observation is that the path loss, in the tunnel environment, appeared to be independent of distance. We observed that multipath components appeared regularly in the delay profiles, which can be understood due to the regularly installed structural objects, such as overhead power line equipment installed along the track.**

***Index Terms*—mmWave, HST, measurement, tunnel, viaduct.**

I. Introduction

High-speed vehicular communications, e.g., high-speed train (HST) communications, will be a promising application for 5G and beyond wireless communication systems [1]. Recently, a high-speed railway scenario was included in deployment scenarios for the next generation access technologies in the 3rd Generation Partnership Projects (3GPP) [2]. It is expected that HST communications will support not only control and safety applications but also various high data-rate applications, e.g., access to multimedia services. These can be achieved by utilizing millimeter-wave (mmWave) frequency bands for HST [3].

To develop and evaluate mmWave HST communication systems, it is crucial to have knowledge of the propagation characteristics. So far, mmWave propagation characteristics have been intensively investigated for urban micro-/macro-cell and indoor scenarios [4]–[7]. Unlike the sub-6 GHz bands that have been comprehensively investigated in the literature [8]–[11], only a few studies have investigated mmWave HST communication channels [12] [13]. For instance, the authors of [9] and [10] performed HST channel measurements in rural and station environments at sub-6 GHz bands, characterized channel parameters such as path loss, K-factor, delay spread, and etc. The work in [12], based on mmWave channel measurements in a tunnel scenario, investigated channel characteristics for various HST scenarios by using extensive ray-tracing (RT) simulations. Furthermore, existing channel models rarely support mmWave HST scenarios. The WINNER II channel model [14] for sub-6 GHz bands can provide a moving network scenario for HST in a rural area.

HST propagation scenarios can be generally classified into the following scenarios: open space, viaduct, cutting, hilly terrain, tunnels, and stations [15]. However, more than one HST scenario may exist in a shot range, considering the complex environments along the railway. An example is a mixed environment of tunnel and viaduct, in that viaducts are typically used between tunnels in mountain areas. This mixed environment of the HST scenarios has proven to be a challenging task in channel measurements and analysis [16].

We conducted HST channel measurements in a tunnel and viaduct scenario at 28 GHz and investigated the propagation characteristics of a high-mobility channel. We considered a 3GPP-like HST deployment scenario where base stations (or remote radio heads, RRHs) are linearly positioned along the tracks, and a relay is mounted on the roof of a train carriage [2]. In the measurements, the base station acts as a transmitter (TX) and the relay as a receiver (RX). While conducting the measurements, the RX was traveling at a speed up to 170 km/h.

The organization of the rest of the paper is as follows. Section II describes the measurement campaign, such as the measurement equipment and scenarios. Section III presents the measurement data analysis results. Conclusive remarks are given in Section IV.

II. Measurement campaign

A. Measurement Equipment

A measurement campaign was conducted using a wideband mmWave band exploration channel sounder (mBECS), which was developed by ETRI (Electronics and Telecommunications Research Institute, Korea) [6]. The center frequency is 28 GHz and the maximum bandwidth is 500 MHz. The sounder collects complex channel impulse responses (CIRs) to investigate propagation characteristics, such as path loss, delay spread, Doppler shift, and its statistics. To do this, we used a pulse compression technique based on the periodic transmission of a pseudo-noise (PN) sequence with a length of 4095 in the time domain, while maintaining synchronization between a TX and an RX.

Figure 1 depicts the channel sounder used for the HST channel measurements. As shown in Figure 1, it consists of several modules, e.g., a baseband module (BBM), a transceiver module (TRXM), a power module, and a timing module (TIM). These modules can be used both in TX and RX. Therefore, a TX includes an RF up-converter module (RFM) and a TX antenna. Similarly, an RX includes an RF down-converter module and RX antenna.

We used a directional antenna with a 12.6 dBi gain and 30° half-power beamwidth (HPBW) both in azimuth and elevation domain for the TX to enlarge the measurement coverage area. At the RX side, a monopole-type omnidirectional antenna with a 4 dBi gain was used to collect data for path loss, delay spread, and Doppler shift. The RX antenna pattern was designed to consider a typical vehicle-to-infrastructure (V2I) scenario where the TX antenna is typically positioned above the RX antenna.

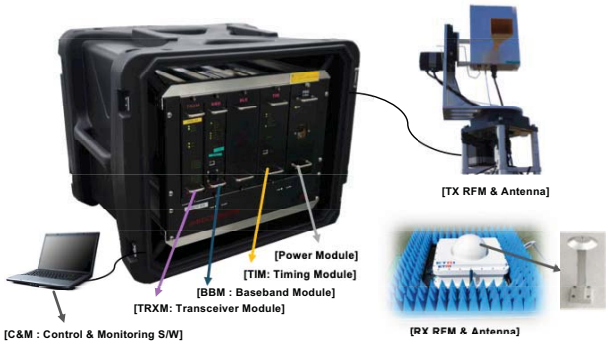

Fig. 1. The channel sounder used in the measurements

B. Measurement Scenarios

A measurement campaign was conducted in a railway test track located parallel to a commercial railway in Osong, Korea. Owned by the Korean government and operated by the Korea Railroad Research Institute (KRRI), the 13-kilometer track comprises high-speed sections (speeding up to 230 km/h), sharp curves, slopes, nine bridges (or viaducts), and six tunnels for performance tests.

Figure 2 shows the measurement environment. The measurement was conducted in a high-speed section for a 450 m distance range. There are two propagation scenarios: viaduct scenario (segment A) and tunnel scenario (segment B). As shown in Figure 2, the distance between the TX and the tunnel entrance, which is segment A, is about 179 m, and the length of the tunnel (test tunnel #4), which is segment B, is 271 m.

The train used in the measurement is the so-called HEMU train (High-speed Electric Multiple Unit), provided by the KRRI, shown in Figures 2 and 3. The total length of the HEMU is about 150 m. There are two electric locomotives at the front and the back of the train that can move both directions. During the measurement campaign, the maximum speed of the train was 170 km/h. For the measurements, as shown in Figure 3, the RFM and the RX antenna were installed

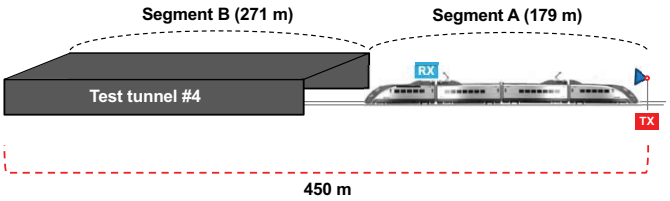

(a) Sketch of the HST measurement scenario

(b) Photograph of the HST measurement scenario

Fig. 2. HST measurement environments

on the rooftop of the train carriage, and the other parts were placed inside the train carriage. The height of the RX antenna was 4.5 m above the ground. We placed the TX antenna next to the test track as shown in Figure 4 (We utilized a custom-built sturdy antenna master to endure the wind blast from a high-speed train.) and set the antenna boresight towards the tunnel.

During the measurement campaign, there were steel structures, including overhead line equipments along the test track, to provide electricity to a train (see Figures 2 and 4). As shown in Figure 3, there were pantographs on the rooftop of the test train, which can act as scatterers. It should be noted that there were no other moving objects in the HST measurement. Since the train moves at such high speeds, the measurement campaigns were conducted in a manner to minimize the possibility of traffic accidents. By using a jig, we secured the RFM and the RX antenna onto the train rooftop. We also mounted a radom upon the RX antenna to mitigate the effects of wind for the high-speed moving train. Furthermore, absorbers were attached around the receiving antenna to reduce the influence of reflected waves caused by the train's roof.

III. Data Analysis Results

A. Path Loss

The path loss is an important parameter which can describe the large-scale effects of the propagation channel. We analyzed the measurement data based on the alpha-beta(AB) model [5]. The AB model is given by

$$\mathrm{PL}_{AB}(d) = 10\alpha \log_{10}(d) + \beta + X_\sigma \quad (1)$$

where d is the distance from TX to RX, α is the slope, β is the floating offset value, and X_σ is the log-normal shadow

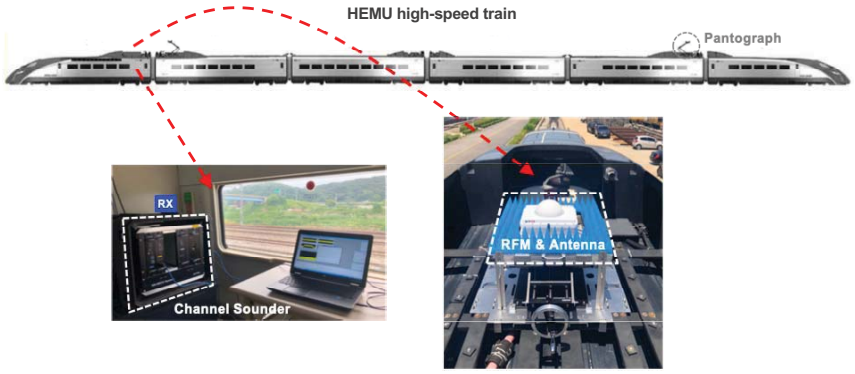

Fig. 3. RX measurement setup

Fig. 4. TX measurement setup

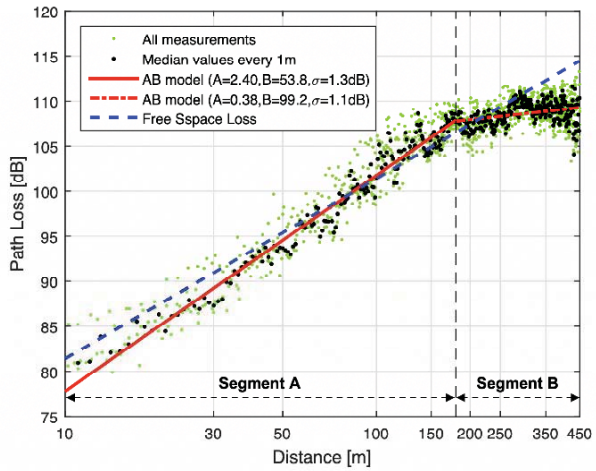

Fig. 5. Path loss results

fading (SF) factor parameterized by the SF standard deviation σ.

With (1), we obtain α and β by using the least-squares fitting. In our fitting, we sub-sampled all the measurement data at every 1 m interval by calculating the local median. Figure 5 shows the measured PL result and the AB model in the HST scenario. In the figure, the dashed line at around 180 m indicates the location of the tunnel entrance. Since the measured PL have significantly different patterns in segment A and B, we estimate α and β separately for segment A and B. As described in the previous section, segment A is viaduct scenario and segment B is tunnel scenario. The path loss exponent of Segment A is 2.4, which is slightly higher than the free space model. We think that this is due to the similar antenna heights of the TX and the RX, and the effect of the train carriage's roof. The path loss exponent of Segment B is 0.38, which implies that the PL is almost constant with respect to distance. This seems to be due to the "waveguide effect" in the tunnel.

The SF is assumed to be modeled as a zero-mean Gaussian random variable with standard deviation σ as follows;

$$X_\sigma = N(0, \sigma^2) \tag{2}$$

The SF parameter can be estimated by deviations of the measured PL data from the fitting model. Figure 6 shows the probability density function (PDF) of the SF for segments A and B from the HST measurements. We also plot Gaussian PDF with the estimated standard deviation σ. It is observed that the measured SF and the the Gaussian fit are in good agreement.

B. Power delay profile and delay spread

Power delay profile (PDP) provides the intensity of a signal received through a multipath channel as a function of time delay. Figure 7 illustrates representative concatenated PDPs in the HST scenario for a distance range of 450 m. In the figure, the horizontal axis, the vertical axis, and the colour code denote the propagation delay, the TX-RX distance, and the received power in dB, respectively. Furthermore, white dashed-line in the figure indicates the locations of the tunnel entrance.

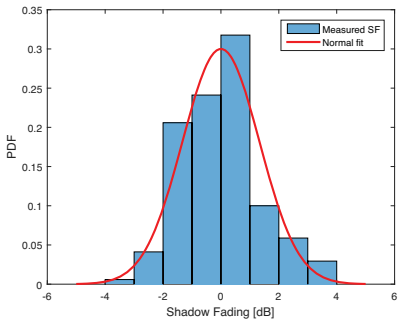

(a) Segment A (viaduct scenario)

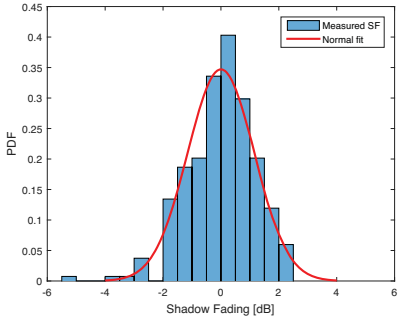

(b) Segment B (tunnel scenario)

Fig. 6. PDFs of shadow fading

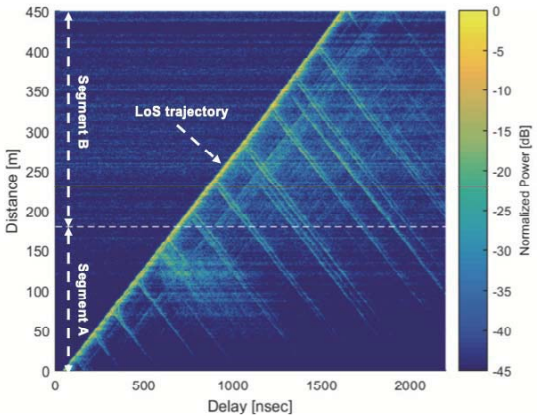

Fig. 7. Illustration of concatenated power delay profiles

It can be observed from Figure 7 that there are multiple trajectories in the distance-delay domain. For both segments, the LoS propagation trajectory can be observed in the figure. From Figure 7, we can observe that: (1) There are many trajectories starts regularly from the LoS trajectory. These components were associated with the overhead power line equipments along the test track. (2) There are several parallel trajectories with the LoS trajectory. It may be caused by objects on the roof of the test train, such as pantographs. (3) Before entering the tunnel, there are many multipaths in a 70–150 m distance range and 600–1100 nsec delay range. Those are generated from structures in the entrance of the tunnel. (4) Due to reflections from the tunnel walls, there are many multipaths in the tunnel as well.

The root-mean-square (RMS) delay spread (DS) is an important parameter characterizing the temporal dispersive properties of multipath channels. The RMS delay spread (σ_{DS}) was calculated from the measured PDPs as follows:

$$\sigma_{\mathrm{DS}} = \sqrt{\frac{\sum_{l=1}^{L}(\tau_l - \bar{\tau})^2 \cdot P_l}{\sum_{l=1}^{L} P_l}} \tag{3}$$

where τ_l and P_l denote the delay and power of the l-th multipath, respectively, $l \in [1, ..., L]$ with L representing the total number of multipaths. Moreover, the average delay ($\bar{\tau}$) is given by

$$\bar{\tau} = \sqrt{\frac{\sum_{l=1}^{L}\tau_l \cdot P_l}{\sum_{l=1}^{L} P_l}} \tag{4}$$

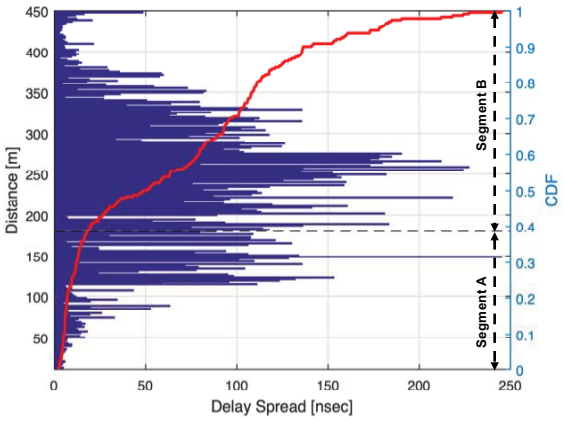

Fig. 8. RMS delay spreads and their CDF

The threshold was set to 20 dB from the peak component to determine effective multipath components. Figure 8 illustrates RMS delay spreads and the resulting cumulative distribution functions (CDFs) for the HST scenario. In the figure, the blue bar, solid red line denote the RMS delay spread values and their CDFs, respectively. The delay spread values are considerably large in most cases except for short or long distances. From Figure 8, we can observe the following characteristics: (1) Even though, for the viaduct scenario (segment A), the delay spread value increases at the tunnel entrance. (2) In the tunnel scenario (segment B), the delay spread has the greatest value in the middle of the tunnel and decreases towards the end of the tunnel.

C. Doppler shift

Figure 9 depicts exemplary Doppler spectra from the HST measurement data. To estimate the Doppler shift, a time interval of 660 consecutive channel impulse responses (CIRs) (corresponding to 21.6 msec), chosen to satisfy the sampling-theorem condition, is used. By applying a discrete Fourier

transform (DFT) to the measured CIRs with respect to time, we can estimate the Doppler shift [17]. To reduce the level of the sidelobes, the Blackman window is applied prior to the DFT operation. This gives the power delay-Doppler profile (PDDP) where each delay component is associated with its own Doppler shift, as shown in Figure 9 (a). The Doppler spectrum can be obtained by summing the magnitude squared values of PDDP over the delay domain as in Figure 9 (b).

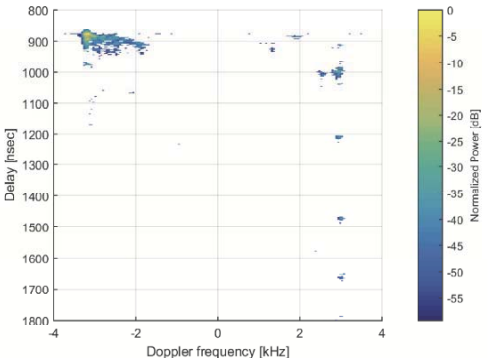

(a) PDDP

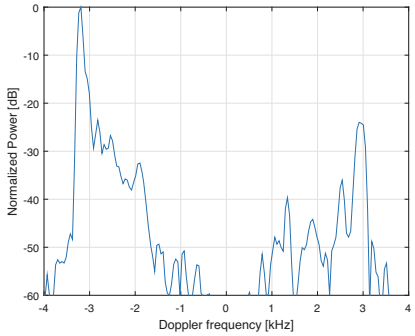

(b) Doppler spectrum

Fig. 9. Illustration of power delay-Doppler profile and Doppler spectrum

In the HST scenario, there are only two main Doppler components, as in Figure 9. There is an LoS propagation component at around -3.2 kHz (the RX was moving away from the TX), and the second component can be found at 3 kHz, which is opposite to the LoS component. However, the second component was periodically observed in the delay domain. It is caused by the overhead power line equipment is installed periodically along the test track.

IV. Conclusion

Utilizing a channel sounder at 28 GHz with a 500 MHz bandwidth, 3GPP-like HST measurements were performed in a high-speed train test track. During the measurements, a receiver was traveling at a speed up to 170 km/h for the high-speed train scenario. Based on the measurement data, we investigated the propagation characteristics such as path loss, delay spread and Doppler shift. It will be helpful for the design of 5G mobile communication systems based on mmWave bands in high-mobility environments.

Acknowledgment

This work was supported by Institute for Information & communications Technology Promotion (IITP) grant funded by the Korean government (MSIT) [2017-0-00066, "Development of time-space based spectrum engineering technologies for the preemptive using of frequency"][2017-0-01973, "(Korea-Japan) International collaboration of 5G mmWave based Wireless Channel Characteristic and Performance Evaluation in High Mobility Environments"].

References

[1] ITU-R, "IMT Vision – Framework and overall objectives of the future development of IMT for 2020 and beyond," *ITU-R Recommendation M.2083*, Sep. 2015.

[2] 3GPP, "Study on Scenarios and Requirements for Next Generation Access Technologies," *TR 38.913*, 2017.

[3] K. Guan, B. Ai, B. Peng, D. He, G. Li, J. Yang, Z. Zhong, and T. Kürner, "Towards realistic high-speed train channels at 5G millimeter-wave bandpart I: paradigm, significance analysis, and scenario reconstruction," *IEEE Transactions on Vehicular Technology*, vol. 67, no. 10, pp. 9112–9128, 2018.

[4] X. Wu, Y. Zhang, C.-X. Wang, G. Goussetis, el Hadi M. Aggoune, and M. M. Alwakeel, "28 GHz indoor channel measurements and modeling in laboratory environment using directional antennas," *Proceeding of European Conference of Antenna and Propagation (EuCAP)*, April 2015.

[5] S. Sun, T. S. Rappaport, S. Rangan, T. A. Thomas, A. Ghosh, I. Z. Kovacs, I. Rodriguez, O. Koymen, A. Partyka and J. Jarvelainen, "Propagation path loss models for 5G urban micro- and macro-cellular scenarios," *in submitted to IEEE VTC2016-Spring*, 2016.

[6] J. Lee, J. Liang, M.-D. Kim, J.-J. Park, B. Park, and H. K. Chung, "Measurement-Based Propagation Channel Characteristics for Millimeter-Wave 5G Giga Communication Systems," *ETRI Journal*, vol. 38, no. 6, pp. 1031–1041, 2016.

[7] S. Hur, S. Baek, B. Kim, Y. Chang, A. F. Molisch, T. S. Rappaport, K. Haneda, and J. Park, "Proposal on millimeter-wave channel modeling for 5G cellular system," *IEEE Journal of Selected Topics in Signal Processing*, vol. 10, no. 3, pp. 454–469, 2016.

[8] K. Guan, Z. Zhong, B. Ai, and T. Kürner, "Semi-deterministic path-loss modeling for viaduct and cutting scenarios of high-speed railway," *IEEE Antennas and Wireless Propagation Letters*, vol. 12, pp. 789–792, 2013.

[9] T. Zhou, C. Tao, S. Salous, L. Liu, and Z. Tan, "Channel characterization in high-speed railway station environments at 1.89 GHz," *Radio Science*, vol. 50, no. 11, pp. 1176–1186, 2015.

[10] T. Domínguez-Bolaño, J. Rodríguez-Piñeiro, J. A. García-Naya, and L. Castedo, "Experimental characterization of LTE wireless links in high-speed trains," *Wireless Communications and Mobile Computing*, vol. 2017, 2017.

[11] S.-d. Li, Y.-j. Liu, L.-k. Lin, Z. Sheng, X.-c. Sun, Z.-p. Chen, and X.-j. Zhang, "Channel measurements and modeling at 6 GHz in the tunnel environments for 5G wireless systems," *International Journal of Antennas and Propagation*, vol. 2017, 2017.

[12] D. He, B. Ai, K. Guan, Z. Zhong, B. Hui, J. Kim, H. Chung, and I. Kim, "Channel measurement, simulation, and analysis for high-speed railway communications in 5G millimeter-wave band," *IEEE Transactions on Intelligent Transportation Systems*, vol. 19, no. 10, pp. 3144–3158, 2017.

[13] G. Li, B. Ai, D. He, Z. Zhong, B. Hui, and J. Kim, "On the feasibility of high speed railway mmWave channels in tunnel scenario," *Wireless Communications and Mobile Computing*, vol. 2017, 2017.

[14] P. Kyosti and *et al.*, "WINNER II Channel Models," *IST-WINNER II D1.1.2*, Nov. 2007.

[15] C.-X. Wang, A. Ghazal, B. Ai, Y. Liu, and P. Fan, "Channel measurements and models for high-speed train communication systems: A survey," *IEEE communications surveys & tutorials*, vol. 18, no. 2, pp. 974–987, 2016.

[16] B. Ai, R. He, Z. Zhong, K. Guan, B. Chen, P. Liu, and Y. Li, "Radio wave propagation scene partitioning for high-speed rails," *International Journal of Antennas and Propagation*, vol. 2012, 2012.

[17] K.-W. Kim, J.-J. Park, M.-D. Kim, and J. Lee, "Spectral Leakage Reduction of Power-Delay- Doppler Profile for mm-Wave V2I Channel," *Submitted to the 9th International Conference on Information and Communication Technology Convergence*, Oct. 2018.